Available online at www.sciencedirect.com

ScienceDirect

Physics Procedia 10 (2010) 162–167

Physics Procedia

www.elsevier.com/locate/procedia

3rd International Symposium on Shape Memory Materials for Smart Systems

Large Superplastic Strain in Non-Modulated Epitaxial Ni-Mn-Ga Films

S.R. Yeduru[a]*, A. Backen[b], S. Fähler[b], L. Schultz[b], and M. Kohl[a]

[a] *Karlsruhe Institute of Technology, IMT, Hermann-von-Helmholtz-Platz 1, 76344 Eggenstein-Leopoldshafen, Germany*
[b] *IFW Dresden, P.O. Box 270116, 01171 Dresden, Germany*

Abstract

The phase transformation and superplastic characteristics of free-standing epitaxial Ni-Mn-Ga stripes are reported. The stripes are prepared by micromachining a 1 μm thick Ni-Mn-Ga film sputter-deposited on a single crystalline MgO (100) substrate using optical lithography and a Chromium-based sacrificial layer technology. The stripes are oriented at angles of 0 and 45 degrees with respect to the Ni-Mn-Ga unit cell. Electrical resistance versus temperature characteristics reveal a reversible thermally induced phase transformation between 169°C and 191°C. Stress-strain measurements are performed with the stress applied along the $[100]_{Ni\text{-}Mn\text{-}Ga}$ as well as $[110]_{Ni\text{-}Mn\text{-}Ga}$ direction. Depending on the orientation, the twinning stress ranges between 25 and 30 MPa, respectively. For the $[100]_{Ni\text{-}Mn\text{-}Ga}$ and $[110]_{Ni\text{-}Mn\text{-}Ga}$ directions, superplastic behaviour with a strain plateau of 12 % and 4% are observed, respectively, indicating stress-induced reorientation of non-modulated martensite variants.

Keywords: magnetic shape memory films; epitaxial Ni-Mn-Ga films; sacrificial layer technology; superplasticity

1. Introduction

Ferromagnetic shape memory alloys (FSMAs) like Ni-Mn-Ga exhibit large magnetic-field-induced strains in the order of 10 % [1,2]. The underlying physical mechanism is due to magnetic-field induced reorientation (MIR), the so-called magnetic shape memory (MSM) effect being currently under intense investigation worldwide [3]. The key requirements for MIR are ferromagnetic martensites having high magnetocrystalline anisotropy and low twinning stress, which can be obtained most easily in single crystals [1-3]. One focus of research is on the introduction of MSM actuation in small dimensions, where the favourable scaling of energy density and remote controllability by an external magnetic field are of special interest. Recent work demonstrated that epitaxial films are a promising route to fabricate MSM microactuators [4-8]. After deposition, the epitaxial films need to be released from the rigid substrate as the stress range for MSM actuation is limited by the fairly low blocking stress of a few megapascals [9]. Thus, in order to achieve useful deformations, it is essential to develop deposition and substrate-release technologies allowing for free-standing epitaxial FSMA films. Epitaxial films have been successfully deposited on various

* Corresponding author. Tel.: +49 7247822753; fax: +49 7247827798.
E-mail address: srinivasa.yeduru@kit.edu.

1875-3892
doi:10.1016/j.phpro.2010.11.093

substrates, e.g., $SrTiO_3$ (100) [10], MgO (100) [5] and water-soluble NaCl (100) [11]. Though deposition of Ni-Mn-Ga on sacrificial NaCl (100) substrates appears to be quite simple, a NaCl substrate has several disadvantages, such as hygroscopic behaviour and poor adhesion. Recently, we could demonstrate that the deposition of Ni-Mn-Ga on a Chromium buffer is a highly reproducible technology to obtain free-standing Ni-Mn-Ga films [7]. In the following, a fabrication process is presented to obtain free-standing Ni-Mn-Ga stripes by combining optical lithography and a Chromium-based sacrificial layer technology. After discussion of the process flow, the structural properties of the released films will be shown. Then, the phase transformation and direction-dependent superplastic properties will be presented. These experiments are carried out in tensile mode, suitable for films. This is in difference compared to compressive test commonly used for bulk Ni-Mn-Ga [12,13].

2. Fabrication Technology

Ni-Mn-Ga thin films of 1 μm thickness are grown by DC magnetron sputtering on a MgO (100) substrate covered by an epitaxial Chromium buffer layer of 100 nm thickness. The sputtering target is prepared by casting using a target composition of $Ni_{46}Mn_{32}Ga_{22}$. Since martensitic transitions strongly depend on composition, composition adjustment is a challenge, since commonly no stoichiometric transfer from the target to the substrate occurs. Phase formation in the films strongly depends on the chemical composition, which is closely related to deposition temperature [14] and magnetron configuration [15]. In the present case, the deposition temperature is set to 400°C. By adjusting the deposition temperature, phase formation in epitaxial Ni-Mn-Ga films can be controlled [5]. However, if deposition temperature is too low, chemical ordering of Ni-Mn-Ga does not occur and, therefore, the film shows paramagnetic behaviour at room temperature. In difference to bulk, post heat treatment is not suitable for thin films, because it leads to the loss of Mn and Ga and, as a consequence, the formation of a secondary Ni_3Ga phase occurs [16]. Details on the sputtering process can be found in Refs. [11,14,15]. By means of energy-dispersive X-ray spectroscopy (EDX), giving an accuracy of 0.5 at.% when using a $Ni_{50}Mn_{25}Ga_{25}$ standard, the film composition is determined to be $Ni_{50.5}Mn_{30.5}Ga_{19}$.

The as-deposited films are structured to a stripe pattern using optical lithography and wet-chemical etching. The stripes are useful test structures, particularly for tensile experiments. In addition, they facilitate substrate release to further investigate MIR performance. In the present investigation, the Ni-Mn-Ga thin films are patterned at different angles of 0 and 45 degrees with respect to MgO<100> substrate edges. These angles are chosen because of the growth direction of the Ni-Mn-Ga unit cell, which is rotated by 45° relative to the unit cell of the MgO (100) substrate [11]. This orientation is favoured by the low misfit compared to direct, non-rotated epitaxial growth.

In previous work, a number of substrate release technologies have been studied including mechanical peeling, sacrificial layer and sacrificial volume technologies [6,7,11]. In the present investigation, a sacrificial Cr layer is used, which plays a crucial role in epitaxial growth as well as in substrate release. Most importantly, the Cr layer acts as a buffer layer for epitaxial growth allowing sufficient adhesion. In addition, it is a useful sacrificial layer as it can be removed selectively by chemical dissolving. Furthermore, the Cr layer fulfills requirement on low roughness and chemical stability.

The MgO (100) substrate is well suited for deposition of epitaxial Ni-Mn-Ga films, but it is not suitable for applications due to its chemical inertness. Therefore, the Ni-Mn-Ga stripes are released and transferred to a micromachined target substrate consisting of a receiver bonding site and openings to allow for unrestricted motion. For the substrate transfer, a transfer bonding technology has been adopted allowing the handling of delicate films such as epitaxial Ni-Mn-Ga films on the wafer scale [17].

Fig. 1 shows a Ni-Mn-Ga stripe of 10 mm length and 1 mm width after substrate release and transfer bonding. Observations of the surface in the free-standing Ni-Mn-Ga film with Atomic Force Microscopy (Fig. 2) show the twin microstructure, which is oriented by 45 degrees with respect to the substrate edge.

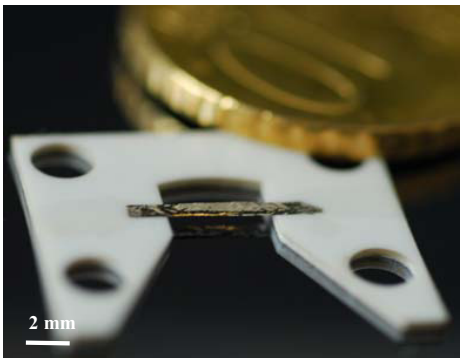

Fig. 1: Ni-Mn-Ga stripe after substrate release and transfer bonding.

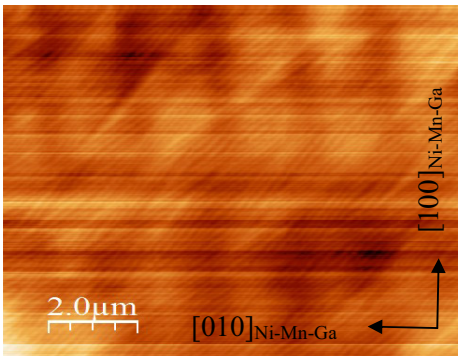

Fig. 2: AFM image of the free-standing Ni-Mn-Ga film. The traces of martensitic twin boundaries with the surface are oriented along a [110] $_{Ni\text{-}Mn\text{-}Ga}$ direction.

3. Structural Properties

The structure of the free-standing Ni-Mn-Ga films has been analyzed by X-ray diffraction (wavelength λ = 1.54 Å). Fig. 3 shows an X-ray diffractogram obtained in Bragg Brentano geometry. The observed high intense peaks are from the ceramic substrate where the free standing film was mounted in bridge shape and the Ni-Mn-Ga film peak intensities are rather low due to the wavy surface of the free-standing films. The intense peak at 2θ = 54.3° is attributed to the reflection from non-modulated (NM) martensite. In addition, a peak at 2θ = 58.6° of lower intensity is observed, which is attributed to (400) 14M martensite. The spectrum shows no reflections from the Cr layer indicating that the sacrificial layer is completely dissolved.

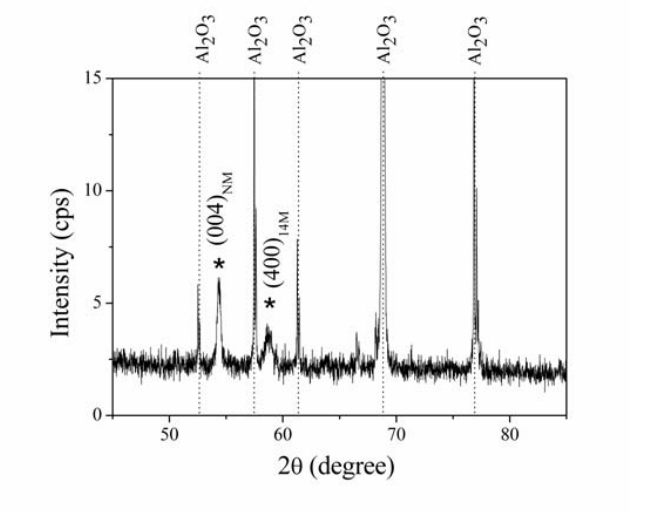

Fig. 3: θ -2θ X-ray diffractogram in Bragg-Brentano geometry of a free-standing Ni-Mn-Ga film of 1 µm thickness.

In previous investigations, it has been shown that 14M is a nanotwinned NM martensite phase and the microstructural transition between both phases proceeds by coarsening of twin boundaries [18]. A key conclusion from these experiments is that films on a rigid substrate more easily form a modulated phase compared to bulk. For free-

standing films, however, we expect a different behaviour: neither stress induced martensite helps to increase the martensitic transformation temperature nor the constraint of a rigid substrate hinders detwinning from 14M to NM.

4. Thermally-induced phase transformation properties

The phase transformation temperatures of free-standing Ni-Mn-Ga stripes are investigated by four-probe electrical resistance measurements. The experiments are performed in a thermostat allowing precise control of ambient temperature. The temperature is ramped step-wise through the phase transformation regime and the corresponding change of electrical resistance is monitored until stationary equilibrium conditions are reached. Fig. 4 shows a typical electrical resistance characteristic.

Upon heating, we observe the austenite start temperature at A_s = 182°C and the corresponding finish temperature at A_f = 191°C. Upon cooling, martensite formation starts at M_s = 179°C and ends at M_f = 169°C, respectively. It has been shown that the phase transformation temperatures of off-stoichiometric Ni-Mn-Ga alloys strongly depend on electron concentration [19]. While for films on substrates often the stress between both increases the martensitic transformation temperature significantly [20], this can be excluded in the present case since no external stress is present in a freestanding film [11, supplementary]. However, these results are in line with results on NM martensite in bulk Ni-Mn-Ga single crystals [21]. The observed phase transformation temperatures are a characteristic feature of NM crystal structure, which is in line with X-ray diffraction results as shown in Figure 3.

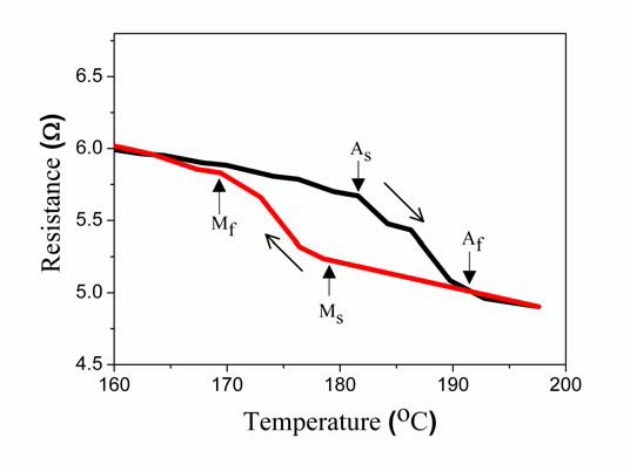

Fig. 4: Electrical resistance characteristic of a free-standing Ni-Mn-Ga stripe of 1 μm thickness measured along $[110]_{Ni\text{-}Mn\text{-}Ga}$ direction.

5. Mechanical Properties

The free-standing Ni-Mn-Ga stripes are investigated by tensile experiments in displacement-control mode using a strain rate of 0.01 mm/min. The tensile load is applied along [100] and [110] crystallographic direction of the Ni-Mn-Ga films. The width and length of the Ni-Mn-Ga test specimens are 1 and 10 mm, respectively. Fig. 5 shows typical engineering stress-strain curves for a tensile load applied along the [100] and [110] direction of the Ni-Mn-Ga film. In both cases, a broad strain plateau is observed after an initial elastic mechanical response. While in bulk often a steplike increase of stress level is observed during an intermartensitic transition from 14M to NM, this is not the case during the present experiments. This indicates that due to the coexistence of 14M and NM in the present samples, no nucleation barrier hinders the coarsening process from nanotwinned 14M to macrotwinned NM.

The twinning stress is determined by the tangential method and is about 25 MPa for $[100]_{Ni\text{-}Mn\text{-}Ga}$ orientation. Most strikingly, we observe a large superplastic behaviour with a strain plateau of 12 % indicating stress-induced reorientation of the NM martensite variants. Obviously, the films can hold very large stress values above 200 MPa

showing no brittle behaviour like polycrystals. For $[110]_{Ni\text{-}Mn\text{-}Ga}$ orientation, a different mechanical behaviour is observed. In this case, a higher twinning stress of about 30 MPa is found and a considerably smaller strain plateau of 4 % occurs.

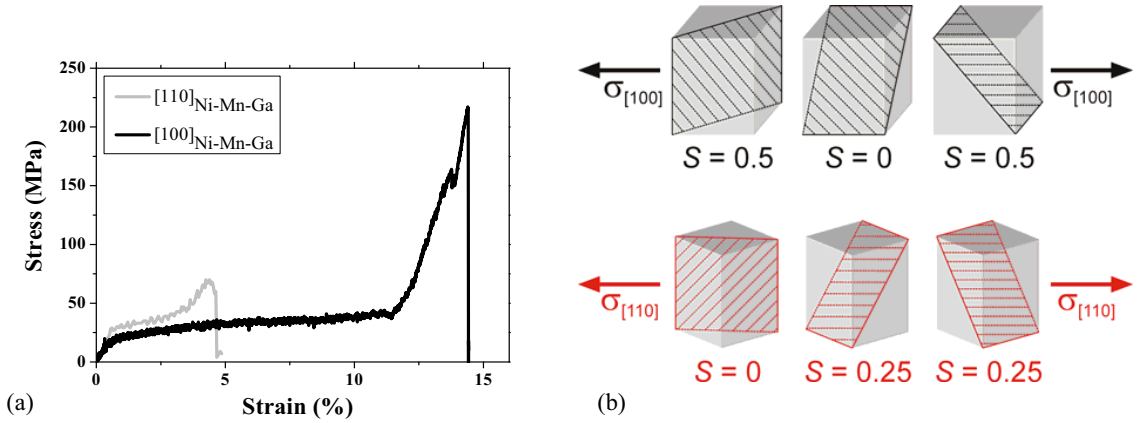

Fig. 5: Tensile stress-strain characteristics of free-standing epitaxial Ni-Mn-Ga stripes of 1 µm thickness along the [100] and [110] crystallographic direction of Ni-Mn-Ga as indicated in (a). (b) Possible orientations of {110} planes in a cubic unit cell and the Schmid factors *S* for both stress directions.

As NM martensite exhibits a higher c/a ratio than 14M it can compensate more strain. In previous studies, the lattice constants of the NM structure have been determined to be a = b = 5.46 Å and c = 6.76 Å, which gives an upper limit of strain of |1-c/a| = 23% [7]. As the Ni-Mn-Ga stripes have not been subjected to mechanical loading or a magnetic field, we can assume that they are in a multi-variant state before straining. For tensile loading in [100] direction, variants with the long c-axis orientation along the loading direction do not contribute. Thus, the maximum strain is given by the fraction of variants with a-axis orientation along the loading direction, which is estimated from the experiment to be about 50%. For tensile loading in [110] direction, the maximum strain is expected to be lower since only the projection of the [100] direction onto the loading direction is relevant. Further microstructural investigations on the fractions of contributing variants in initial state will be required for a quantitative understanding.

The difference in twinning stress for tensile loading along the [100] and [110] directions of the Ni-Mn-Ga unit cell can be explained by analyzing the shearing stress which acts on the twin boundaries following the concept of Otsuka and Wayman [22]. The stress necessary to shear two {110} type twin boundaries is equal to $\tau_{\{110\}} = \sigma \cdot S$ with σ being the external stress and the Schmid factor *S* [23]. The Schmid factor is a geometrical factor and can be calculated from $S = \cos\lambda \cdot \cos\kappa$, with λ and κ being the angles between the external stress direction and the shearing direction and the normal of the {110} plane, respectively. Consequently, σ is only dependent on the Schmid factor $\sigma = \tau_{\{110\}}/S$. The slid system consisting of {110} planes and the corresponding <110> shearing direction with high values of *S* are expected to be activated first whereas slid systems with $S = 0$ are not activated at all. We calculated *S* for the different {110} planes and their corresponding shearing direction for the case of a cubic unit cell (Fig. 5b). The approximation shows that for tensile loading along $[100]_{Ni\text{-}Mn\text{-}Ga}$, the Schmid factor is twice as high than along $[110]_{Ni\text{-}Mn\text{-}Ga}$. From this one would expect a factor two difference between the twinning stress when loading in [100] and [110] directions. The experimentally observed difference is smaller (25 and 30 MPa). The tetragonal distortion of the martensite results in angular deviation from the cubic approximation used here. In case of the [100] direction this results in a reduction of *S* from the maximum value of 0.5, while for the [110] direction *S* may increase for some tilt and rotation.

5. Conclusions

Free-standing epitaxial Ni-Mn-Ga stripes are fabricated by sputter-deposition of a 1 μm thick Ni-Mn-Ga film on a single crystalline MgO (100) substrate and subsequent micromachining using optical lithography and a Chromium-based sacrificial layer technology. The Ni-Mn-Ga stripes are oriented along the different crystallographic directions allowing direction-dependent tensile measurements after substrate release. X-ray diffraction results on the free standing films show major contributions of NM and minor contributions of 14M martensite. The NM structure is also reflected in the high phase transformation temperatures observed by electrical resistance measurements. For the [100] and [110] directions, the tensile measurements reveal superplastic behaviour with a strain plateau of 12% and 4%, respectively, indicating stress-induced reorientation of NM martensite starting from a multi-variant initial state. Due to the NM structure, a rather high twinning stress of 25 and 30 MPa is observed for the $[100]_{\text{Ni-Mn-Ga}}$ and $[110]_{\text{Ni-Mn-Ga}}$ directions, respectively. The orientation dependence of twinning stress can be qualitatively explained by the different orientations of external tensile load with respect to the twinning planes.

6. Acknowledgments

The authors would like to thank Harald Leiste for support in XRD measurements at the IMF-I and Berthold Krevet for useful discussions. The presented work receives research funding from the Deutsche Forschungsgemeinschaft (DFG) and is part of the priority program SPP1239.

References

1. K. Ullakko, J.K.Huang, C. Kantner, R.C. O'Handley, and V.V. Kokorin, *Appl. Phys. Lett.* 69 (1996) 1966.
2. A. Sozinov, A. Likhachev, N. Lanska, K.Ullakko, *Appl. Phys. Lett.* 80 (2002) 1746-1748.
3. For a recent review, see. e.g., O. Söderberg, Y. Ge, A. Sozinov, S.P. Hannula and V.K Lindroos, *Smart Materials and Structures* Vol. 14, 5, (2005) 223-235.
4. J. W. Dong, J. Q. Xie, J. Lu, C. Adelmann, C. J. Palmstrøm, J. Cui, Q. Pan, T. W. Shield, R. D. James, S. McKernan, *J. Appl. Phys*. 95(5) (2004) 2593-2600.
5. M. Thomas, O. Heczko, J. Buschbeck, U.K. Rößler, J. McCord, N. Scheerbaum, L. Schultz and S. Fähler, *New J. of Phys.* 10 (2008) 23040.
6. F. Khelfaoui, M. Kohl, B. Buschbeck, O. Heczko, S. Fähler, and L. Schultz, *Eur. Phys. J. Special Topics*, 158, (2008) 167-172.
7. A. Backen , S.R. Yeduru , M. Kohl , S. Baunack, A. Diestel , B. Holzapfel, L. Schultz, S. Fähler, *Acta Materialia* 58 (2010) 3415–3421.
8. M. Kohl**,** S.R.Yeduru, F. Khelfaoui, B. Krevet, A. Backen, S. Fähler, T. Eichhorn, G. Jakob and A. Mecklenburg, *Materials Science Forum* Vol. 635 (2010) 145-154.
9. S.J. Murray, M. Marioni, S.M. Allen, R.C. O'Handley, T.A. Lograsso, *Appl. Phys. Lett.* 77, 886 (2000)
10. O. Heczko, M. Thomas, J. Buschbeck, L. Schultz, and S. Fähler, *Appl. Phys. Lett.* 92, (2008) 072502.
11. M. Thomas, O. Heczko, J. Buschbeck, Y. W. Lai, J. McCord, S. Kaufmann, L. Schultz, S. Fähler, *Advanced Materials* 21 (2009) 3708.
12. V. A. Chernenko, A. Amengual, E. Cesari, V. V. Kokorin, I. K. Zasimchuk, *Journal de Physiqe* IV C2(5) (1995) C2-95.
13. P.Müllner, V. A. Chernenko and G. Kostorz, *Scripta Materialia*, 49(2) (2003) 129-133.
14. S. Fähler, O. Heczko, M. Thomas, R. Niemann, J. Buschbeck, L. Schultz, Proc. ACTUATOR'08, H. Borgmann Ed., (2008) 754-757.
15. S. Kaufmann, J. Buschbeck, O. Heczko, L. Schultz, S. Fähler, Proc. ICOMAT'08, to be published.
16. A. Backen, R. Niemann, S. Kaufmann, J. Buschbeck, L. Schultz, S. Fähler, ESOMAT (2009) 04002.
17. T. Grund, R. Guerre, M. Despont and M. Kohl, *Eur. Phys. J. Special Topics* 158 (2008) 237-242.
18. S. Kaufmann, U. Rößler, O. Heczko, M. Wuttig, J. Buschbeck, L. Schultz, S. Fähler, *Phys. Rev. Lett.* 104 (2010) 145702.
19. V.A. Chernenko, E. Cesari, V.V. Khovailo, I.N. Vitenko, *Scr. Metall. Mater.* 33 (1995) 1239.
20. M. Thomas, O. Heczko, J. Buschbeck, L. Schultz, S. Fähler, *Appl. Phys. Lett*. 92 (2008) 192515.
21. N. Lanska, O. Söderberg, A. Sozinov, Y. Ge, K. Ullakko, V.K. Lindroos, *J. Appl. Phys*. 95 (2004) 8074.
22. K. Otsuka, C.M. Wayman (ed.), Shape Memory Materials,1st Edition, Cambridge University Press 1998.
23. G. Gottstein: Physikalische Grundlagen der Materialkunde, 3rd Edition, Springer 2007.